ELSEVIER

Computers and Chemical Engineering 26 (2002) 1265–1279

Computers & Chemical Engineering

www.elsevier.com/locate/compchemeng

The need for using rigorous rate-based models for simulations of ternary azeotropic distillation

P.A.M. Springer, S. van der Molen, R. Krishna *

Department of Chemical Engineering, University of Amsterdam, Nieuwe Achtergracht 166, 1018 WV Amsterdam, The Netherlands

Received 24 September 2001; received in revised form 18 March 2002; accepted 18 March 2002

Abstract

Experiments were carried out in a bubble cap distillation column operated at total reflux with the system: water–ethanol–methylacetate. This system has two binary azeotropes (water–ethanol and water–methylacetate), which gives a simple distillation boundary connecting the two azeotropes. All experiments were restricted to the homogenous region without liquid phase splitting. For certain starting compositions the measured distillation composition trajectories clearly demonstrate that crossing of the distillation boundary is possible. In order to rationalize our experimental results, we develop a rigorous nonequilibrium (NEQ) stage model, incorporating the Maxwell–Stefan diffusion equations to describe transfer in either fluid phase and a fundamental description of tray hydrodynamics. The developed NEQ model anticipates the boundary crossing effects, and is in excellent agreement with a series of experiments carried out in different composition regions. In sharp contrast, an equilibrium (EQ) stage model fails even at the *qualitative* level to model the experiments. The differences in the NEQ and EQ trajectories emanates from differences in the component Murphree efficiencies, which in turn can be traced to differences in the binary pair vapor phase diffusivities $Đ_{y,ij}$. It is concluded that for reliable design of azeotropic distillation columns we must take interphase mass transfer effects into account in a rigorous manner.

Keywords: Azeotropic distillation; Residue curve maps; Rate-based models; Maxwell–Stefan equations; Distillation boundary; Nonequilibrium stage; Equilibrium stage

Nomenclature

a'	interfacial area per unit volume of vapor bubbles ($m^2\ m^{-3}$)
B_{ij}	NRTL parameters; see Table 1 (K)
c_i	molar concentration of species i ($mol\ m^{-3}$)
c_t	mixture molar density ($mol\ m^{-3}$)
d_b	bubble diameter (m)
D_{12}	Fick diffusivity in binary mixture ($m^2\ s^{-1}$)
$Đ_{ij}$	Maxwell–Stefan diffusivity for pair i–j ($m^2\ s^{-1}$)
E_i^{MV}	component Murphree point efficiency, dimensionless
Fo	Fourier number, $Fo \equiv 4Đ_y\tau_V/d_b^2$, dimensionless
G_{ij}	NRTL parameters; see Table 1, dimensionless
g	acceleration due to gravity ($m\ s^{-2}$)
h	distance along froth height (m)
h_f	height of dispersion (m)
$\mathbf{J}_i$	molar diffusion flux of species i relative to the molar average reference velocity $\mathbf{u}$ ($mol\ m^{-2}\ s^{-1}$)

* Corresponding author. Fax: +31-20-52-55604.
E-mail address: krishna@science.uva.nl (R. Krishna).

0098-1354/02/$ - see front matter
PII: S0098-1354(02)00039-X

k_{ij} element for matrix of multicomponent mass transfer coefficient (m s^{-1})
$[k]$ matrix of multicomponent mass transfer coefficients (m s^{-1})
$[K_{eq}]$ diagonal matrix of K-values, dimensionless
$[K_{Oy}]$ matrix of multicomponent overall mass transfer coefficients (m s^{-1})
$\mathbf{N}_i$ molar flux of species i (mol m^{-2} s^{-1})
$\mathbf{N}_t$ mixture molar flux (mol m^{-2} s^{-1})
$[NTU_{Oy}]$ matrix of overall number of vapor phase transfer units, dimensionless
n number of diffusing species, dimensionless
S parameter defined in Eq. (20) (m s^{-1})
Sh Sherwood number, dimensionless
t_c liquid-bubble contact time (s)
T temperature (K)
$\mathbf{u}_i$ velocity of the diffusing species i (m s^{-1})
$\mathbf{u}$ molar average mixture velocity (m s^{-1})
V_b single bubble rise velocity (m s^{-1})
x_i liquid composition for component i, dimensionless
y_i vapor composition for component i, dimensionless

Greek

α_{ij} non-randomness parameter in NRTL equation, see Table 1, dimensionless
κ_{ij} binary Maxwell–Stefan liquid mass transfer coefficients (m s^{-1})
ρ_L density of the liquid (kg m^{-3})
μ_L liquid viscosity (Pa s)
μ_i molar chemical potential (J mol^{-1})
σ surface tension (N m^{-1})
τ_V vapor phase residence time (s)
τ_{ij} NRTL parameters; see Table 1, dimensionless
ξ dimensionless distance along dispersion or column height, dimensionless

Subscript

b referring to a bubble
f referring to the froth
i component index
j stage index
Oy overall parameter referred to the vapor phase
ref reference
t referring to total mixture
x referring to the x phase (liquid)
y referring to the y phase (vapor)

Superscript

M referring to Murhpree
L referring to the liquid phase
V referring to the vapor phase
* referring to equilibrium state

1. Introduction

Traditionally chemical engineers have developed their design procedures for separation and reaction equipment using Fick's law of diffusion as a basis. For a two-component system Fick's law postulates a linear dependence of the molar diffusion flux of component 1, $\mathbf{J}_1$, defined with respect to the molar average mixture reference velocity $\mathbf{u}$, and its composition gradient ∇x_1:

$$\mathbf{J}_1 \equiv c_1(\mathbf{u}_1 - \mathbf{u}) = -c_1 D_{12} \nabla x_1 \tag{1}$$

For component 2, a similar relation holds:

$$\mathbf{J}_2 \equiv c_2(\mathbf{u}_2 - \mathbf{u}) = -c_1 D_{21} \nabla x_2 \tag{2}$$

Since mole fractions of the two components sum to unity, i.e. $x_1 + x_2 = 1$, the mole fraction gradients sum to zero, i.e. $\nabla x_1 + \nabla x_2 = 0$ and the two molar diffusion fluxes are equal in magnitude but opposite in sign:

$$\mathbf{J}_1 + \mathbf{J}_2 \equiv 0; \qquad \mathbf{J}_1 = -\mathbf{J}_2 \tag{3}$$

Consequently there is only one independent Fick diffusivity $D_{12}(= D_{21})$ and for distillation of binary

mixtures there is only one independent Murphree point efficiency, that is equal for both components 1 and 2:

$$E_1^{MV} = \frac{y_{1,L} - y_{1,E}}{y_1^* - y_{1,E}} = \frac{y_{2,L} - y_{2,E}}{y_2^* - y_{2,E}} = E_2^{MV} \quad (4)$$

where the subscripts E and L refer to the conditions entering and leaving a vertical zone on a distillation tray, respectively; see Fig. 1. The Murhpree point efficiency E_1^{MV} is bounded between 0 and 1 (Lockett, 1986; Taylor and Krishna, 1993). The situation changes dramatically for multicomponent mixtures, i.e. when the number of components n is three or more; there is no requirement that the Murphree point efficiencies E_i^{MV} be equal to one another:

$$E_1^{MV} \neq E_2^{MV} \neq E_3^{MV} \ldots\ldots \neq E_n^{MV} \quad (5)$$

or that they be bounded. There is a large body of experimental evidence for ternary distillation in the published literature to verify that component efficiencies are not equal to one another and that any of these efficiencies could vary from $-\infty$ to $+\infty$; see the comprehensive literature survey given in Chapter 13 of Taylor and Krishna (1993).

For the calculation of interphase mass transfer fluxes in multicomponent mixtures, it is now generally accepted that we need to adopt the Maxwell–Stefan diffusion formulation for either fluid phase; the recent review by Krishna and Wesselingh (1997) presents several examples to support this contention. In the Maxwell–Stefan diffusion formulation, chemical potential gradients are used as the driving forces for diffusion

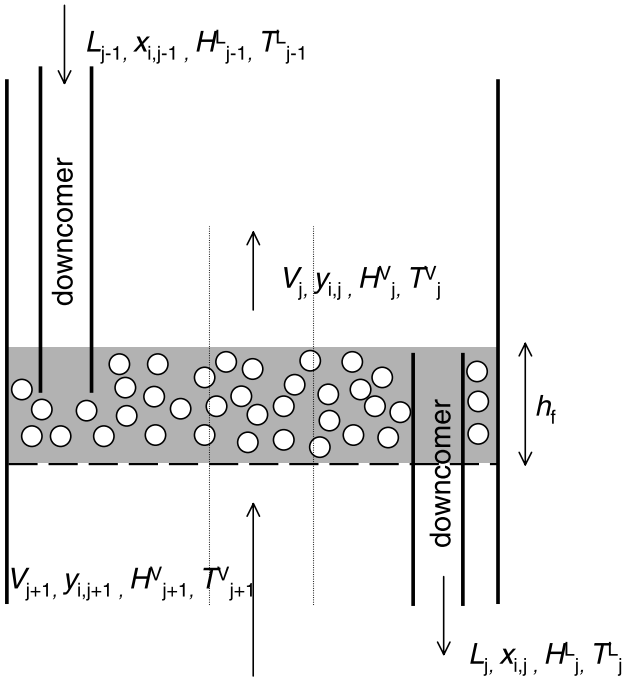

Fig. 1. Schematic of the bubble froth regime on the tray.

and a linear relation is postulated between the driving forces and the fluxes in the form:

$$-\frac{x_i}{RT}\nabla\mu_i = \sum_{\substack{j=1 \\ j\neq i}}^{n} \frac{x_j\mathbf{J}_i - x_i\mathbf{J}_j}{c_t Đ_{ij}} = \sum_{\substack{j=1 \\ j\neq i}}^{n} \frac{x_j\mathbf{N}_i - x_i\mathbf{N}_j}{c_t Đ_{ij}}; \quad i = 1,2,\ldots,n \quad (6)$$

where the molar fluxes $\mathbf{N}_i$ in a laboratory-fixed coordinate reference frame are defined by

$$\mathbf{N}_i \equiv c_i u_i;$$

$$\mathbf{N}_i \equiv \mathbf{J}_i + x_i\mathbf{N}_t \quad \mathbf{N}_t = \sum_{i=1}^{n} \mathbf{N}_i; \quad i = 1,2,\ldots,n \quad (7)$$

The $Đ_{ij}$ in Eq. (6) are the Maxwell–Stefan diffusivities; these are equal to the Fick diffusivities only for ideal gas mixtures.

The Maxwell–Stefan formulation, based on the thermodynamics of irreversible processes, takes proper account of diffusional 'coupling' between the species transfers i.e. the flux of any species depends on the driving forces of all the species present in the mixture. In a distillation column, the influence of species coupling manifests itself in significant differences in the component Murphree efficiencies E_i^{MV}. For simulation of multicomponent distillation columns, containing either trays or packings, the Maxwell–Stefan formulation has been incorporated into commercially available software packages such as RATEFRAC (marketed by Aspen Technology) and CHEMSEP (available through the CACHE corporation; see also www.chemsep.org). Such simulation models are usually called *rate-based* or *nonequilibrium* (NEQ) models to distinguish these from the classical approaches using the *equilibrium* (EQ) stage models.

Pelkonen, Kaesemann and Gorak (1997) performed total reflux experiments with the system methanol–2-propanol–water in a packed distillation column and showed that if the composition at the top of the column is located on a distillation boundary the experimentally measured composition profiles end up with a reboiler composition that is rich in water, whereas the EQ model predicts that the reboiler composition corresponds to pure 2-propanol!; see Fig. 2. The NEQ model is able to describe the experimentally observed profile quite well. Similar dramatic differences between the predictions of the EQ and NEQ models were also obtained for the system acetone–methanol–2-propanol–water when the composition near the top of the column is chosen to lie on a distillation boundary.

The experimental results of Pelkonen et al. (1997) raise the question whether the observed dramatic differences between NEQ and EQ model predictions are also obtained when the starting compositions are not located precisely on the distillation boundary but on either side of it. The major objective of our paper is to demonstrate that distillation boundaries can be crossed

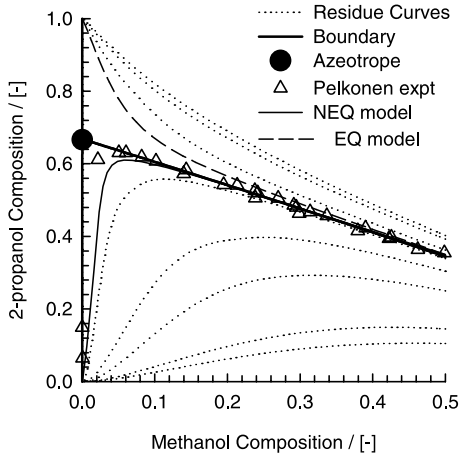

Fig. 2. Composition trajectories for distillation of methanol–2-propanol–water. Measurements of Pelkonen et al. (1997) in a 0.1 m diameter column packed with Sulzer BX packing and operating at total reflux. Also shown are simulation results using the NEQ and EQ models. The dotted lines represent the residue curves.

Table 1
NRTL parameters for binary mixtures at 101.3 kPa, taken from Gmehling & Onken (1977)

Component I	Component j	B_{ij} (K)	B_{ji} (K)	α_{ij} (−)
Water	Ethanol	624.917	−29.169	0.294
Water	Methylacetate	796.817	334.671	0.35
Ethanol	Methylacetate	198.971	134.162	0.3
Water	Methanol	594.630	−182.605	0.297
Water	2-Propanol	729.221	70.662	0.288
Methanol	2-Propanol	65.711	−89.743	0.304

These parameters are used along with $G_{ij} = \exp(-\alpha_{ij}\tau_{ij})$ and $\tau_{ij} = B_{ij}/T$.

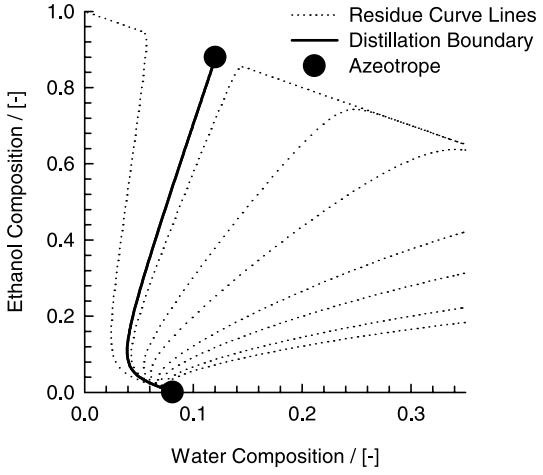

Fig. 3. Residue curve map for the water (1)–ethanol (2)–methylacetate (3) system, showing a curved distillation boundary and two binary azeotropes between water–ethanol and water–methylacetate.

provided that the starting compositions are located within a finite region of compositions on one side of the distillation boundary. Furthermore, we aim to show that such boundary crossing phenomena can be predicted by the NEQ models and can be attributed to differences in component Murphree efficiencies. Clearly, the EQ models are incapable of anticipating boundary crossing effects since the EQ distillation trajectories must necessarily follow the residue curve maps for total reflux operations (Stichlmair & Fair, 1998).

To verify the boundary crossing phenomena, we performed experiments with the system water–ethanol–methylacetate in a bubble cap tray distillation column. The residue curve map for this system, calculated with NRTL parameters listed in Table 1, is shown in Fig. 3. This system shows two binary azeotropes between the water–ethanol and water–methylacetate mixtures; a slightly curved distillation boundary connects the two azeotropes. For high water compositions there is a region of partial miscibility and our experimental work was restricted to water mole fractions below 0.2.

2. Experimental set-up

The experiments were carried out in a laboratory-scale distillation column supplied by Schott Nederland B.V.; see Fig. 4. The double layered glass column with vacuum between the inner and outer shell contains a total condenser (stage 1), a partial reboiler (stage 12) and ten equal bubble cap trays (stages 2–11) for which the dimensions are tabulated in Table 2 and pictured in Fig. 5. The distillation column is divided into two sets of five bubble cap trays by an intersection at which a continuous feed can be introduced to the column. Product streams can be tapped automatically from the condenser and manually from the reboiler. The glass distillation column has several small openings of 10 mm in diameter, which are sealed with Teflon-coated septums. These opening enable liquid and vapor samples to be withdrawn by means of a syringe. The column has a total height of 2160 mm and a 50 mm inner diameter.

The reboiler is placed in a heating mantle, which is connected with a PC provided with the required software (Honeywell: WINNT-workstation 4.0; FIX MMI V 6.15/75-I/O-points runtime; OPTO CONTROL rel.2.2a). By means of the PC, the reboiler temperature can be controlled as well as the feed- and product-flows. Furthermore, it provides an automatic safety shut down in case the column reboiler accidentally tends to dry up. The condenser is connected with a water tap, which supplies cooling water to the glass cooling tubes inside the condenser.

Experiments under total reflux conditions and atmospheric pressure were carried out with the system water–ethanol–methylacetate. For any given experiment, eight vapor and four liquid samples were taken from

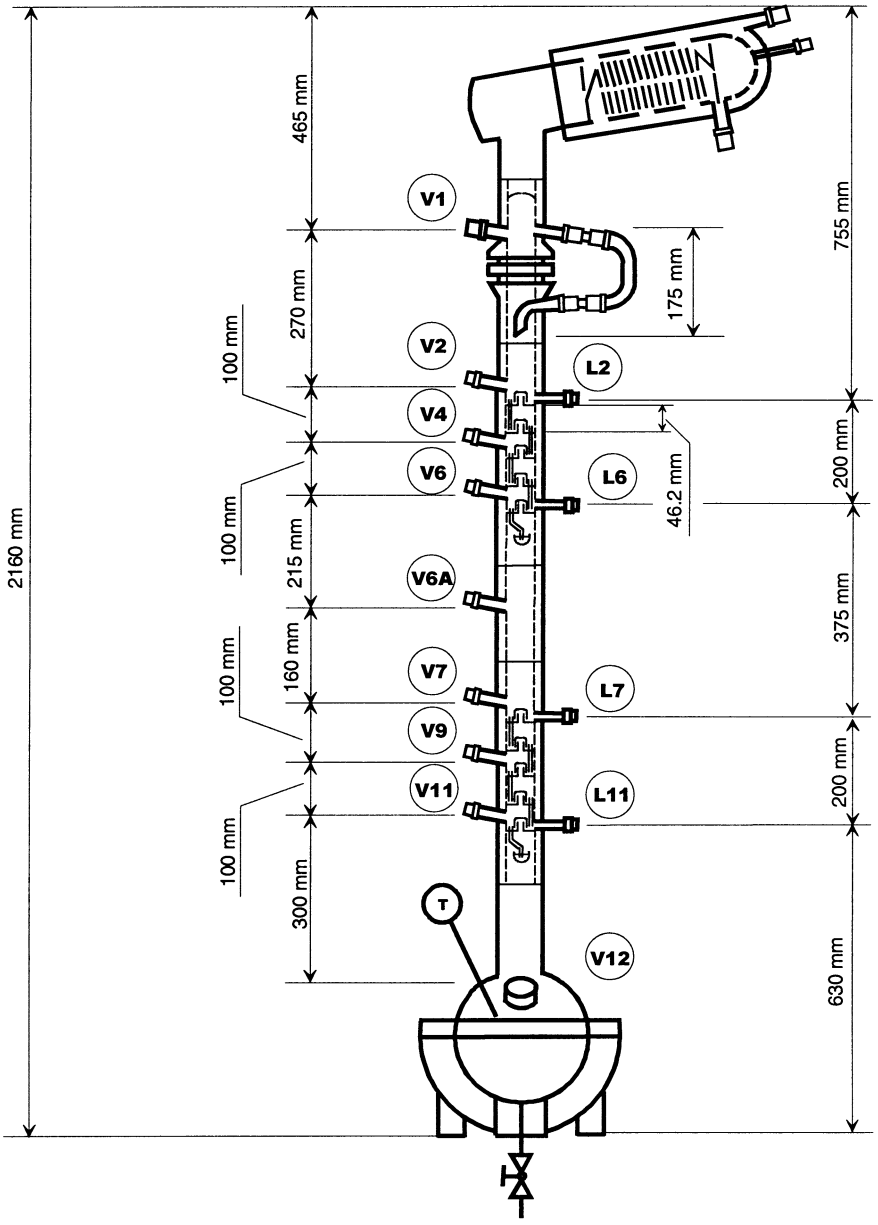

Fig. 4. Schematic of laboratory-scale distillation column. Includes total condenser (1), partial reboiler (12), ten bubble cap trays (2-11) and 13 draw-off faucets, nine for vapor samples (V) and four for liquid samples (L).

Table 2
Bubble cap tray design of the laboratory-scale distillation column

Column diameter	0.0500 m	Hole pitch	0.0142 m
Tray spacing	0.0462 m	Cap diameter	0.0281 m
Number of flow passes	1	Skirt clearance	0.0030 m
Liquid flow path length	0.0308 m	Slot height	0.0050 m
Downcomer clearance	0.0039 m	Active area (of total area)	97.30%
Deck thickness	0.0030 m	Total hole area (of total area)	8.27%
Hole diameter	0.0142 m	Downcomer area (of total area)	1.35%
Weir type	Circular	Slot area	0.000221 m^2
Weir length	0.0182 m	Riser area	0.000158 m^2
Weir height	0.0092 m	Annular area	0.000462 m^2
Weir diameter	0.0058 m		

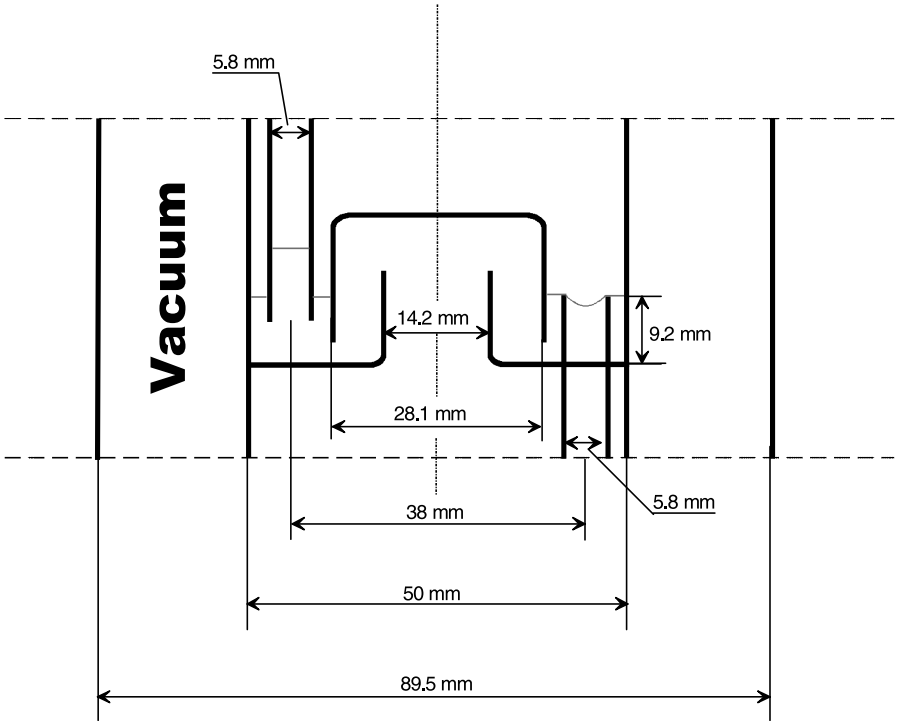

Fig. 5. Details of bubble cap.

several stages (see Fig. 4) and the temperature profile was measured with PT 100 sensors. Each sample volume was intentionally kept small (100 μl) to prevent changes in the composition-profile during the entire experiment. The samples were first dissolved into a reference solvent consisting of 1 vol.% cyclohexane in 99 vol.% acetone before injection into the Gas Chromatograph (type: GC8000-Top with pressure/flow control) by means of an autosampler (type AS800). The channel inside the GC is made of stainless steel and has a total length of 1 m and 0.3175 mm diameter. The carrier gas used was helium because of its high thermal conductivity and chemical inertness. By analyzing samples of pre-prepared, known, compositions, the GC was carefully calibrated. More detailed descriptions of the experimental set-up, measurement technique, GC analysis and composition determination, including pictures of the column and bubble cap trays are available on our web-site: http://ct-cr4.chem.uva.nl/distillation/.

3. Experimental results

The experimentally determined composition trajectories for a set of nine experiments are shown in Fig. 6, along with the residue curve map. For total reflux operation at steady state, the composition of the vapor leaving any given stage equals the composition of the liquid arriving at that stage from above. Therefore, the eight vapor and four liquid composition samples can be combined when plotting the composition trajectories. In Fig. 6 the vapor samples are denoted by open circles and the liquid samples by open squares. The large open circles in Fig. 6 represent the input compositions in the simulations, to be described below. In experiments T3-03, T3-04, T3-10 and T3-11 the column trajectories were all located on the left side of the distillation boundary (indicated by a thick line). All the remaining five experiments clearly exhibit boundary crossing phenomena. We also note that the experimental data points cut across the residue curves to the right at a sharp angle. In all the experiments, there was practically no methylacetate present in the reboiler liquid.

Clearly, boundary crossing phenomena is not in conformity with the assumption of thermodynamic phase equilibrium, which underlies the residue curve maps (Stichlmair & Fair, 1998); this is evidenced by the fact that the experimental trajectories do not follow the residue curve map. In order to understand, and rationalize, the boundary crossing phenomena we apply a rigorous NEQ stage model.

4. Nonequilibrium stage model development

The development of the NEQ stage model follows the ideas and concepts developed earlier by Taylor, Krishna and others and described in earlier publications (Krishna & Wesselingh, 1997; Wesselingh & Kr-

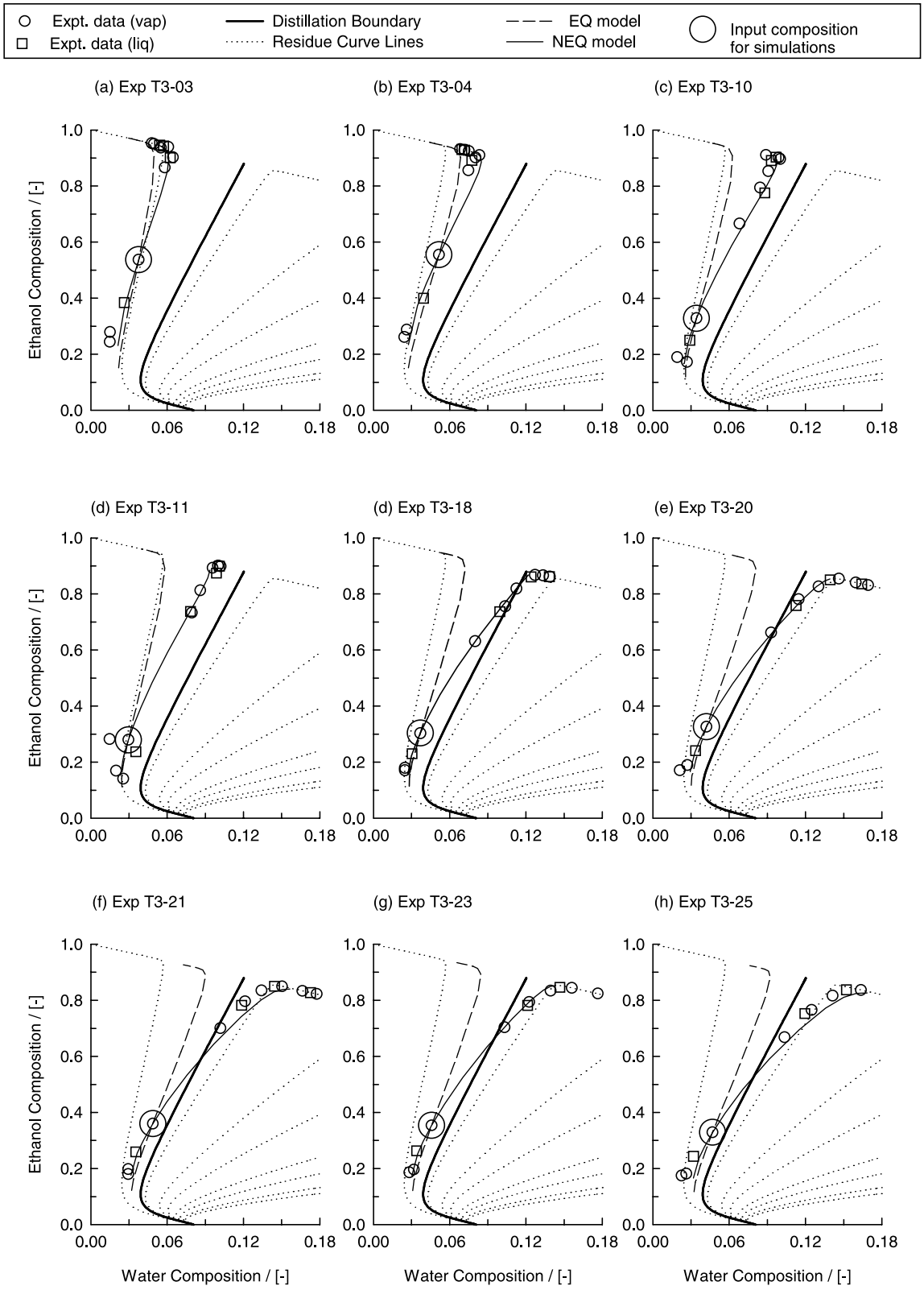

Fig. 6. Experimental results (open circles for vapor samples and open squares for liquid samples) showing the column composition trajectories for the water (1)–ethanol (2)–methylacetate (3) system. Also shown are the simulation results showing the trajectories calculated by the EQ stage model and the NEQ stage model, along with the residue curve map. The large open circles represent the experimental composition specified in the simulations. In the NEQ model simulations a bubble size $d_b = 5.0$ mm was chosen.

ishna, 2000; Taylor & Krishna, 1993; Krishnamurthy & Taylor, 1985; Taylor, Kooijman & Hung, 1994; Baur, Taylor, Krishna & Copati, 1999). The building blocks of the NEQ model are material balances, energy balances, equilibrium relations, and mass and energy transfer models.

We focus first on the material balances and estimation of mass transfer coefficients. Consider first a single stage j pictured in Fig. 1. All our experiments were carried out in the bubbly froth regime. Visual observations of tray operation (photographs are available at our website: http://ct-cr4.chem.uva.nl/distillation) showed that the bubbles were roughly of uniform size and shape. In our model development, we assume that the bubbles rise through the liquid in a plug flow manner. Furthermore, we assume that the liquid phase is well-mixed. The steady state component molar balance for three-component distillation in tray columns is given by the two-dimensional matrix relation

$$V_b \frac{d(y)}{dh} = [K_{Oy}](y^* - y)a' \tag{8}$$

where a' is the interfacial area per unit volume of the dispersed bubble phase and V_b is the bubble rise velocity. Eq. (8) can be re-written in terms of the overall number of transfer units for the vapor phase, $[NTU_{Oy}]$:

$$\frac{d(y)}{d\xi} = [NTU_{Oy}](y^* - y), \tag{9}$$

where $\xi = h/h_f$ is the dimensional distance along the froth and $[NTU_{Oy}]$ is defined as:

$$[NTU_{Oy}] \equiv \int_0^{h_f} \left[[K_{Oy}] \frac{a'}{V_b} \right] dh \tag{10}$$

Carrying out the integration, assuming that the matrix of overall mass transfer coefficients $[K_{Oy}]$ does not vary along the froth height, we obtain

$$[NTU_{Oy}] \equiv [K_{Oy}]a'h_f/V \equiv [K_{Oy}]\ a'\tau_V \tag{11}$$

Assuming that the $[NTU_{Oy}]$ on a single stage is constant, Eq. (9) can be integrated using the boundary conditions

$$\xi = 0(\text{inlet to tray})(y) = (y_{j+1})$$
$$\xi = 1(\text{outlet of tray})(y) = (y_j) \tag{12}$$

to obtain the compositions leaving the distillation stage; detailed derivations are available in Taylor and Krishna (1993):

$$(y^* - y_j) = \exp[-[NTU_{Oy}]](y^* - y_{j+1}) \tag{13}$$

Introducing the matrix $[Q] \equiv \exp[-[NTU_{Oy}]]$, we may re-write Eq. (13) in the form

$$(y_j - y_{j+1}) = [[I] - [Q]](y^* - y_{j+1}), \tag{14}$$

where $[I]$ is the identity matrix. The limiting case of the EQ stage model is obtained when the mass transfer coefficients in either fluid phase attain large values; $[Q]$ reduces in this case to the null matrix and the compositions leaving the tray (y_L) are equal to (y^*), in equilibrium with the liquid leaving the tray. We follow the procedure of Kooijman and Taylor (1995) for implementation of the Eq. (14) in the stage-to-stage calculation.

4.1. Estimation of interfacial areas and mass transfer coefficients

In our model, we assume that all the bubbles to be spherical in shape with a diameter d_b. The interfacial area per unit volume of vapor a' is therefore given by:

$$a' = \frac{6}{d_b} \tag{15}$$

The vapor residence time is determined by:

$$\tau_V = \frac{h_f}{V_b}, \tag{16}$$

where h_f is the height of dispersion (froth). The height of the dispersion on the tray is taken to be the height of the downcomer tube above the tray floor, i.e. 9.2 mm as seen in Fig. 5. This is a good approximation; any uncertainties in the value of h_f will be reflected in the choice of the choice of the bubble size. The bubble rise velocity V_b is estimated using the Mendelson (1967) equation, recommended by Krishna, Urseanu, van Baten and Ellenberger (1999):

$$V_b = \sqrt{\frac{2\sigma}{\rho_L d_b} + \frac{g d_b}{2}}, \tag{17}$$

The overall matrix of mass transfer coefficients $[K_{Oy}]$ is given by the addition of resistances formula:

$$[K_{Oy}]^{-1} = [k_y]^{-1} + \frac{c_t^V}{c_t^L}[K_{eq}][k_x]^{-1}, \tag{18}$$

in which $[K_{eq}]$ represents the diagonal matrix of K-values and $[k_y]$ and $[k_x]$ are the partial transfer coefficient matrices for the vapor and liquid phases, respectively.

Let us consider the matrix of the multicomponent vapor mass transfer coefficient $[k_y]$. The four elements $k_{y,ij}$ can be estimated from the mass transfer coefficients of the constituent binary pairs, $\kappa_{y,ij}$ by making use of the Maxwell–Stefan formulation (Eq. (6)); the final result is:

$$k_{y,11} = \frac{\kappa_{y,13}(y_1\kappa_{y,23} + (1-y_1)\kappa_{y,12})}{S}$$
$$k_{y,12} = y_1\kappa_{y,23}\frac{(\kappa_{y,13} - \kappa_{y,12})}{S}$$
$$k_{y,21} = y_2\kappa_{y,13}\frac{(\kappa_{y,23} - \kappa_{y,12})}{S}$$
$$k_{y,22} = \frac{\kappa_{y,23}(y_2\kappa_{y,13} + (1-y_2)\kappa_{y,12})}{S} \tag{19}$$

where

$$S = y_1\kappa_{y,23} + y_2\kappa_{y,13} + y_3\kappa_{y,12} \tag{20}$$

For each of the binary pairs in the mixture, the $\kappa_{y,ij}$ can be estimated from the following equation for instationary diffusion within a spherical bubble (Taylor & Krishna, 1993):

$$Sh_{ij} \equiv \frac{\kappa_{y,ij} d_b}{Đ_{y,ij}} = \frac{2}{3}\pi^2 \left(\frac{\sum_{m=1}^{\infty} \exp\{-m^2\pi^2 Fo_{ij}\}}{\sum_{m=1}^{\infty} \frac{1}{m^2} \exp\{-m^2\pi^2 Fo_{ij}\}} \right); \quad ij = 12, 13, 23 \tag{21}$$

For Fourier numbers $Fo_{ij} \equiv 4Đ_{y,ij}\tau_V/d_b^2$ larger than about 0.06, the Sherwood number reduces to the asymptotic value:

$$Sh_{ij} = \frac{2\pi^2}{3} \approx 6.58; \quad ij = 12, 13, 23 \tag{22}$$

For this steady-state limit, the binary vapor mass transfer coefficients are given by:

$$\kappa_{y,ij} = \frac{2\pi^2}{3}\frac{Đ_{y,ij}}{d_b} \tag{23}$$

Eq. (23) leads to the important conclusion that $\kappa_{y,ij}$ would have an unity-power dependence on the vapor diffusivity $Đ_{y,ij}$, which is in sharp contrast with the square-root dependence for small values of *Fo*, small vapor phase residence times.

The matrix of the multicomponent liquid mass transfer coefficient $[k_x]$ can be obtained analogously to Eqs. (19) and (20). The binary liquid mass transfer coefficient $\kappa_{x,ij}$ can be obtained from the penetration model:

$$\kappa_{x,ij} = 2\sqrt{\frac{Đ_{x,ij}}{\pi t_c}}, \tag{24}$$

where the contact time of the liquid with gas bubbles, t_c is given by:

$$t_c = \frac{d_b}{V_b} \tag{25}$$

In the above set of model equations, the only unknown parameter is the bubble diameter d_b. Once the bubble diameter is set, the system of equations can be solved. Substituting Eq. (18) in Eq. (11) gives us the $[NTU_{Oy}]$, required for calculation of the $[Q]$ matrix in Eq. (14).

The material balance relations outlined above need to be solved along with the enthalpy balance relations, as described in Chapter 14 of Taylor and Krishna (1993). The required heat transfer coefficients in the vapor phase are calculated from the heat transfer analog of Eq. (21) for the vapor phase Nusselt number. Similarly, the liquid phase heat transfer coefficient is obtained by the application of the penetration model to the liquid phase, analogous to Eq. (24).

The entire set of material and energy balance equations, along with the interphase mass and energy transfer rate relations are then incorporated into a rigorous stage-to-stage model as described in Chapter 14 of Taylor and Krishna (1993). This chapter contains more exhaustive details of this model including sample calculations for binary and ternary mixtures.

5. Simulation strategy

Simulations of the total reflux experimental runs were carried out using both the EQ stage model and the rigorous NEQ stage model developed above. The operating pressure for all experiments was 101.3 kPa and the ideal gas law was used. Activity coefficients were calculated using the NRTL interaction parameters, specified in Table 1, and the vapor pressures were calculated using the Antoine equations. The vapor phase was assumed to be thermodynamically ideal. The column consists of 12 stages, including the total condenser (stage 1) and partial reboiler (stage 12). The reflux flow rate (0.006 mol s^{-1}) and the bottom flow rate (0.0 mol s^{-1}) were used for specifying the column-operations. Since the mass and heat transfer coefficients are independent on the internal flows, the composition and temperature profiles are not dependent on the precise value of the specified reflux flow rate.

Since the column is operated at total reflux, the reflux flow rate determined the inner flow rates of vapor and liquid phases on each stage. Simulation of total reflux operations is 'complicated' by the fact that there is no feed to the column at steady-state. To overcome this problem we specify one of the experimentally determined compositions of the streams leaving or entering a stage as input parameter. The simulated composition profile of the total reflux run is forced to pass through this specified composition. In all the experiments, we specified the vapor composition leaving stage 4 in performing the simulations. This 'input' composition is indicated by the large open circle in Fig. 6. The entire set of equations system was solved numerically by using the Newton's method (Krishnamurthy & Taylor, 1985; Taylor et al., 1994). The NEQ implementation is available in the software program CHEMSEP, developed by Taylor and others (Taylor & Krishna, 1993; Krishnamurthy & Taylor, 1985; Taylor et al., 1994; Baur et al., 1999). Detailed information on CHEMSEP are available in the recent book by Kooijman and Taylor (2001).

6. Comparison of EQ and NEQ simulations with experiments

All experiments were simulated with the EQ stage model and the rigorous NEQ stage model. Let us

consider one of the experiments (T3-23) in some detail. Fig. 7(a) compares the EQ model with the experimental results. The large open circle represents the vapor composition leaving stage 4; this is specified in the simulations. We note that while the experimental points cross the distillation boundary, the EQ column trajectory does not and remains on the left side of the boundary. The EQ trajectory closely follows the residue curve map, shown in Fig. 3. A further point to note is that while the experimental results show that proceeding down the column (in the direction of the reboiler) the compositions get richer in water, the EQ simulations predict that these trays get progressively richer in ethanol. The NEQ model simulations require specification of the bubble diameter. For a range of bubble diameters 3–5.5 mm, the NEQ trajectories have been plotted in Fig. 7(b). For $d_b = 3$ mm, the NEQ trajectory remains to the left of the distillation boundary and does not cross it. Decreasing the bubble diameter has the effect of increasing the mass transfer coefficient (see Eq. (21)) and makes the NEQ model tend towards the EQ model. To match the EQ trajectory, the bubble size has to be 1.5 mm, or smaller. Conversely, increasing the bubble diameter, decreases the mass transfer coefficient and the NEQ trajectories move away from the EQ trajectory. For $d_b = 4.5$, 5 and 5.5 mm, all three NEQ trajectories cross the boundary. The best agreement with the experiments is obtained with $d_b = 5.0$ mm.

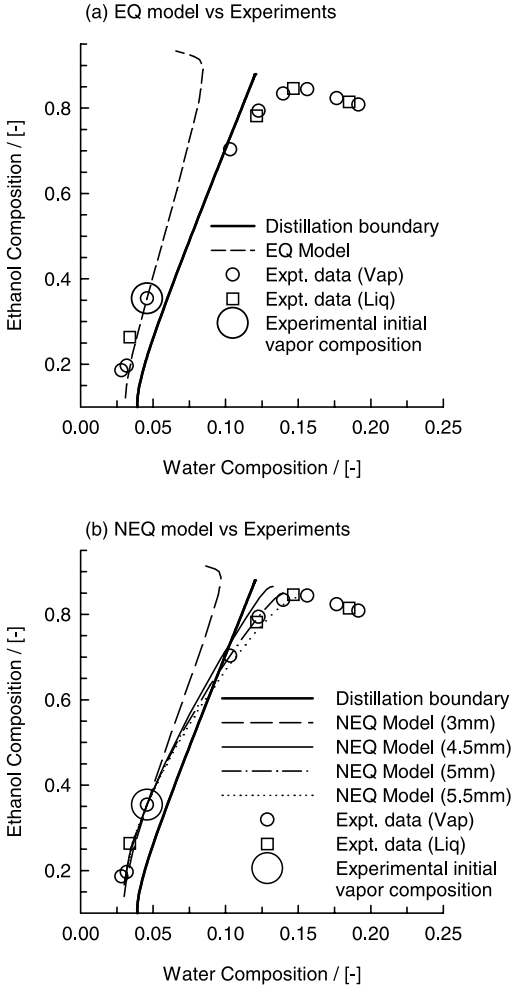

Fig. 7. Simulation results compared with the experimental data (open circles for vapor samples and open squares for liquid samples) for run T3-23. (a) Here the EQ model is compared with experimental results. (b) The NEQ model, for varying bubble diameters is compared with experimental results. The large open circle is the specified composition for the simulations; this corresponds to the vapor composition leaving stage 4.

The simulation results for the EQ and NEQ model, with $d_b = 5.0$ mm, for all the experimental runs are shown in Fig. 6, along with the experimental results.

Consider the runs T3-03, T3-04, T3-10 and T3-11. For all these runs no boundary crossing is observed experimentally; see Fig. 6(a–c). Both EQ and NEQ models do not anticipate boundary crossing. The EQ model follows the trajectory dictated by the residue curve map, whereas the NEQ model has a tendency to cut across to the right of the residue curve. The predictions of the NEQ model are superior to that of the EQ model and are in much better agreement with the experimentally measured composition trajectories. This tendency of the experiments to cut across to the right of the residue curves is strongly evident for run T3-10 and T3-11; here the NEQ model does a very good job of predicting the column trajectory.

Consider the runs T3-18, T3-20, T3-21, T3-23 and T3-25 in Fig. 6. For all these runs we experience boundary crossing and the NEQ model successfully anticipates this phenomenon. In all the cases the EQ model fails to cross the boundary and the EQ trajectory remains on one side of the boundary.

In order to show that the choice of the bubble diameter $d_b = 5.0$ mm is not merely a 'convenient fit' of our ternary experiments, we also carried a set of eight experiments with the binary mixture ethanol–water and sets of four experiments with the binary mixtures water–methanol, water–2-propanol and methanol–2-propanol in the same experimental set-up. The column (vapor) composition trajectories are shown in Fig. 8, along with the NEQ model predictions taking $d_b = 5.0$ mm. The NEQ simulations were carried out by specifying the vapor composition leaving the reboiler (stage 12); as we proceed up the column we approach the azeotropic composition. The NEQ simulations describe the column trajectories very well for all the experimental results.

7. Component Murphree efficiencies in ternary distillation

We may conclude from the foregoing that boundary crossing is caused by *multicomponent* mass transfer

Table 3
Physical and transport properties per stage of experiment T3-23 for the water (1)–ethanol (2)–methylacetate (3) system obtained by NEQ model simulations (bubble diameter = 5.0 mm)

Stage number	$Đ_{y,12}$ (10^{-6} m^2 s^{-1})	$Đ_{y,13}$ (10^{-6} m^2 s^{-1})	$Đ_{y,23}$ (10^{-6} m^2 s^{-1})	$Đ_{x,12}$ (10^{-9} m^2 s^{-1})	$Đ_{x,13}$ (10^{-9} m^2 s^{-1})	$Đ_{x,23}$ (10^{-9} m^2 s^{-1})	σ (10^{-2} N m^{-1})	ρ_L (kg m^{-3})	V_b (m s^{-1})	τ_V (s)	Fo_{12} (−)	Fo_{13} (−)	Fo_{23} (−)
2	19.6	16	7.81	7.62	8.38	4.61	2.484	864	0.190	0.0485	0.152	0.124	0.061
3	19.7	16.1	7.87	7.3	7.64	4.29	2.573	859	0.191	0.0481	0.152	0.124	0.061
4	19.9	16.2	7.93	6.91	6.77	3.91	2.696	853	0.193	0.0477	0.152	0.124	0.061
5	20.1	16.4	8.03	6.46	5.83	3.49	2.864	842	0.195	0.0471	0.151	0.124	0.061
6	20.4	16.7	8.14	6.06	4.95	3.1	3.073	826	0.199	0.0463	0.151	0.124	0.060
7	20.8	16.9	8.28	5.87	4.38	2.86	3.278	806	0.202	0.0455	0.152	0.123	0.060
8	21.1	17.2	8.39	5.92	4.15	2.79	3.424	789	0.205	0.0449	0.153	0.124	0.060
9	21.2	17.3	8.47	6.04	4.1	2.8	3.505	779	0.206	0.0446	0.152	0.123	0.060
10	21.3	17.4	8.5	6.11	4.09	2.81	3.547	774	0.207	0.0444	0.151	0.124	0.060
11	21.4	17.4	8.52	6.13	4.09	2.82	3.572	773	0.207	0.0443	0.152	0.123	0.060

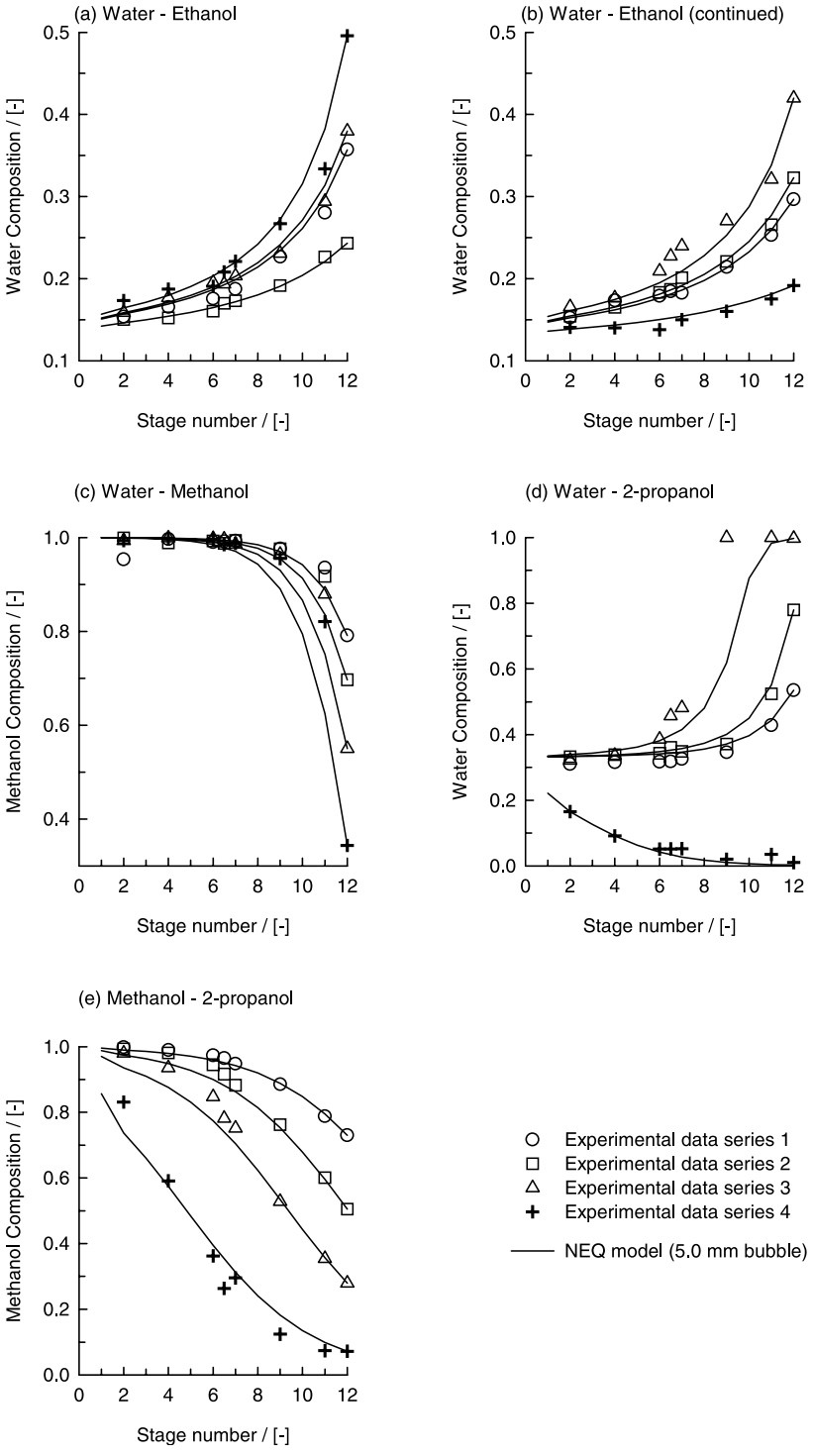

Fig. 8. Experimental results (open circles for vapor samples) showing the column composition trajectories for the water (1)–ethanol (2), water (1)–methanol (2), water (1)–2-propanol (2) and methanol (1)–2-propanol (2) binary systems. Also shown are the simulation results showing the trajectories calculated by the NEQ stage model. For each binary, the experimental vapor composition leaving the reboiler is specified in the simulations. In the NEQ model simulations a bubble size $d_b = 5.0$ mm was chosen.

effects. To explain this in some detail we consider run T3-23. The values of the binary pair vapor diffusivities, $Đ_{y,12}$, $Đ_{y,13}$ and $Đ_{y,23}$ for water (1)–ethanol (2)–methylacetate (3) are specified in Table 3, along with the corresponding liquid phase coefficients. The estimated values of the Fourier numbers calculated using

$$Fo_{ij} = \frac{4Đ_{y,ij}\tau_V}{d_b^2} \tag{26}$$

are also given in Table 3, along with the values of the

surface tension (σ) and liquid density (ρ_L) that are needed in order to estimate the single bubble rise velocity (V_b) and thus the vapor residence time (τ_V) using Eqs. (16) and (17). The vapor phase diffusivities of the three binary pairs are estimated using the Fuller–Schettler–Giddings equation; details of the estimation procedure are to be found in Kooijman and Taylor (2001); this book also specifies the estimation methods for liquid phase diffusivities, densities and surface tension. From Table 3, we see that the *Fo* values exceed 0.06 in all cases, justifying the use of Eq. (22) for estimation of the vapor phase mass transfer coefficients $\kappa_{y,ij}$ of the binary pairs in the mixture; the $\kappa_{y,ij}$ have an unity-power dependence on the vapor diffusivities $Đ_{y,ij}$. By evaluating the individual contributions of the liquid and vapor phases in Eq. (18) it can be verified that the mass transfer resistance is predominantly in the vapor phase. The liquid phase resistance contributes less than 10% of the total resistance; this conclusion was found to be valid for all the nine experimental runs carried out in this study.

To understand the phenomena of boundary crossing, we consider the component Murphree stage efficiencies, defined by

$$E_i^{MV} = \frac{y_{i,L} - y_{i,E}}{y_i^* - y_{i,E}}, \quad i = 1, 2, 3 \tag{27}$$

For the EQ model the component efficiencies are all equal to unity. For the NEQ model the component efficiencies will, in general, differ from one another. To illustrate this, we present the calculations of E_i^{MV} for run T3-23 in Fig. 9 obtained from NEQ simulations with a bubble diameter of 5.0 mm. It is clear the component Murhpree efficiencies are all different from one another and vary from stage to stage. The origin of the differences in E_i^{MV} can be traced to the differences in the binary pair vapor diffusivities, $Đ_{y,12}$, $Đ_{y,13}$ and

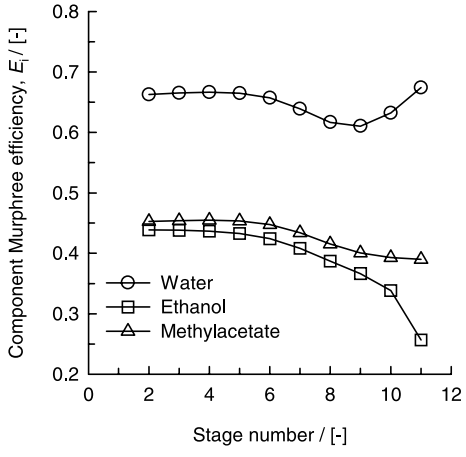

Fig. 9. Component Murphree efficiencies along the column for the experiment T3-23, calculated by the NEQ stage model. In the NEQ model simulations a bubble size $d_b = 5.0$ mm was chosen.

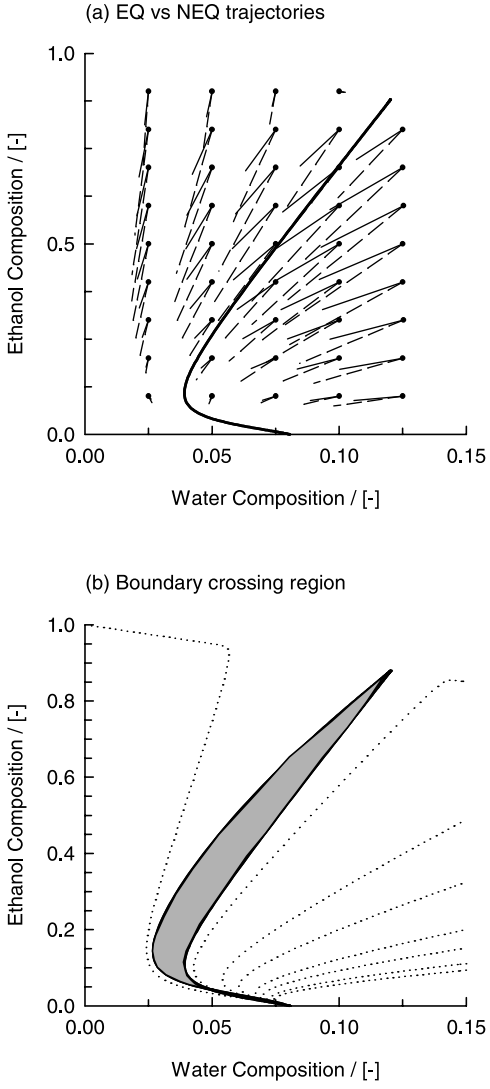

Fig. 10. (a) Calculated direction vectors using the EQ stage model (100% efficiency for all components, denoted by dashed lines) and the NEQ stage model (denoted by continuous lines). In the NEQ model simulations a bubble size $d_b = 5.0$ mm was chosen. (b) All starting compositions within the grey shaded region will cross the distillation boundary to the right of this boundary.

$Đ_{y,23}$. We note that the coefficient $Đ_{y,23}$ is about half of the other coefficients. The difference between binary pair diffusivities cause the component efficiency values to be different from one another. If the binary $Đ_{y,ij}$ were close to one another, the differences in the component efficiencies would be negligible. Differences in the component efficiencies cause the actual composition trajectory followed on any given stage ($y_{i,L} - y_{i,E}$) to deviate from the trajectory dictated by the equilibrium vector ($y_{i^*} - y_{i,E}$).

For various vapor compositions entering any given stage, we have plotted in Fig. 10(a) the actual composition vector ($y_{i,L} - y_{i,E}$), calculated from the NEQ model (taking bubble diameter of 5.0 mm) along with the equilibrium vector ($y_{i^*} - y_{i,E}$). The angle between the

NEQ trajectory (continuous line) and the EQ trajectory (dashed line) increases when the differences in the component efficiencies increase. If all the component efficiencies were equal to one another, the NEQ and EQ trajectories would coincide. We see from Fig. 10(a), that the NEQ trajectory has a tendency to cut across to the right of the EQ trajectory, precisely as has been observed in the experiments (cf. Fig. 6). It is this tendency to cut towards the right of the composition space that causes boundary crossing. By performing several NEQ simulations with various starting compositions of the vapor entering the condenser we can determine the region within which the column trajectories will cross the distillation boundary and end up with reboiler compositions in the region towards the right of the distillation boundary. This boundary crossing region is shown as the grey shaded area in Fig. 10(b). The left face of this grey shaded region defines a boundary that cannot be crossed in practice. It can be verified that the starting compositions for the four runs T3-03, T3-04, T3-10 and T3-11 lie to the left of the grey shaded region; no boundary crossing is therefore observed for these runs. For the remainder of experiments, the starting vapor compositions (leaving stage four), lie within the shaded region; boundary crossing is observed for all the five runs.

8. Conclusions

The following major conclusions can be drawn from the work presented in this paper.

1. The measured composition trajectories during distillation of water–ethanol–methylacetate under total reflux conditions in a bubble cap distillation column clearly demonstrate that crossing of a distillation boundary is possible.
2. An NEQ stage model is able to model the experimental results. The experimental results agree very well with the developed model in which a bubble size of 5.0 mm is chosen. The NEQ model correctly anticipates boundary crossing.
3. An EQ stage model fails to anticipate boundary crossing in any experiment. The EQ model provides a much poorer representation of the column composition trajectories and do not even agree qualitatively with the experimental results. While the experimental trajectory shows that the column gets progressively richer in water as we proceed down to the reboiler, the EQ trajectory predicts that the column gets progressively richer in ethanol; see Fig. 6.
4. The differences in the NEQ and EQ trajectories emanates from differences in the component Murphree efficiencies, which in turn can be traced to differences in the binary pair vapor phase diffusivities $Đ_{y,ij}$.

The overall conclusion to be drawn from this work is that for reliable simulation of distillation of azeotropic systems exhibiting a distillation boundary, we must adopt a rigorous NEQ stage model. In a theoretical simulation study, Castillo and Towler (1998) have shown how the differences in the EQ and NEQ distillation column trajectories could be exploited by the engineer in order to obtain process designs that could not be contemplated if mass transfer effects were ignored, and that some designs based solely on EQ models can become infeasible when mass transfer is considered.

Acknowledgements

The authors acknowledge a grant from the Netherlands Organization for Scientific Research (NWO), Chemical Sciences Division (CW), for investigations on three-phase distillation. The authors are grateful to R. Taylor and H. Kooijman for providing the code to CHEMSEP, which was used in this study after appropriate modification to include the rigid bubble model. R. Baur provided valuable assistance in the development of the NEQ simulation code.

References

Baur, R., Taylor, R., Krishna, R., & Copati, J. A. (1999). Influence of mass transfer in distillation of mixtures with a distillation boundary. *Chemical Engineering Research and Design Trans Industrial Chemistry Engineering*, *77*, 561–565.

Castillo, F. J. L., & Towler, G. P. (1998). Influence of multicomponent mass transfer on homogeneous azeotropic distillation. *Chemical Engineering Science*, *53*, 963–976.

Gmehling, J. L., & Onken, U. (1977). *Vapour–liquid equilibrium data collection*. Frankfurt, Germany: Dechema.

Kooijman, H. A., & Taylor, R. (1995). Modelling mass transfer in multicomponent distillation. *Chemical Engineering Journal*, *57*, 177–188.

Kooijman, H. A., & Taylor, R. (2001). The CHEMSEP book, Libri Books, Books on Demand, Norderstedt, Germany, see also the website: www.chemsep.org.

Krishnamurthy, R., & Taylor, R. (1985). Nonequilibrium stage model of multicomponent separation processes. *American Institute of Chemical Engineers Journal*, *32*, 449–465.

Krishna, R., & Wesselingh, J. A. (1997). The Maxwell–Stefan approach to mass transfer. *Chemical Engineering Science*, *52*, 861–911.

Krishna, R., Urseanu, M. I., van Baten, J. M., & Ellenberger, J. (1999). Wall effects on the rise of single gas bubbles in liquids. *International Communications in Heat and Mass Transfer*, *26*, 781–790.

Lockett, M. J. (1986). *Distillation tray fundamentals*. Cambridge, UK: Cambridge University Press.

Mendelson, H. D. (1967). The prediction of bubble terminal velocities from wave theory. *American Institute of Chemical Engineers Journal*, *13*, 250–253.

Pelkonen, S., Kaesemann, R., & Gorak, A. (1997). Distillation lines for multicomponent separation in packed columns: theory and comparison with experiment. *Industrial and Engineering Chemistry Research*, *36*, 5392–5398.

Stichlmair, J. G., & Fair, J. R. (1998). *Distillation principles and practice*. New York: Wiley-VCH.

Taylor, R., & Krishna, R. (1993). *Multicomponent mass transfer*. New York: Wiley.

Taylor, R., Kooijman, H. A., & Hung, J. S. (1994). A second generation nonequilibrium model for computer-simulation of multicomponent separation processes. *Computers and Chemical Engineering*, *18*, 205–217.

Wesselingh, J. A., & Krishna, R. (2000). *Mass transfer in multicomponent mixtures*. Delft: Delft University Press.